16th European Signal Processing Conference (EUSIPCO 2008), Lausanne, Switzerland, August 25-29, 2008, copyright by EURASIP

HIGH RESOLUTION REDUCED COMPLEXITY SYNCHRONIZATION IN SPREAD SPECTRUM SYSTEMS

Ingmar Groh and Wolfgang Utschick

German Aerospace Center (DLR),
Institute for Communications and Navigation (KN),
82234 Wessling, Germany,
E-mail: Ingmar.Groh@dlr.de

Munich University of Technology (TUM),
Associate Institute for Signal Processing Methods (MSV),
80290 Munich, Germany,
E-mail: utschick@tum.de

ABSTRACT

The estimation of several unknown channel amplitudes and taps in a multipath environment is an important problem when designing receivers both for communication and navigation purposes. A popular approach for these estimation problems are methods solving the maximum likelihood (ML) problem for each dimension separately like the expectation maximization (EM) approach and the more sophisticated space alternating generalized expectation maximization (SAGE) algorithm. However, both methods require a high computational complexity when used in spread spectrum systems due to long spreading sequences. Therefore, we apply methods for decreasing the computational complexity before executing the iterative estimation algorithms. The respective performance is assessed by means of computer simulations for a UMTS scenario which show a negligible degradation in estimation accuracy despite a substantial complexity reduction.

1. INTRODUCTION

The precise and low complex synchronization and channel estimation are important tasks in digital spread spectrum communications systems. More and more applications involve also positioning applications using time of arrival (TOA) or time difference of arrival (TDOA) measurements between the base stations (BSs) and the mobile station (MS). A precise location determination requires therefore the synchronization of the line of sight (LOS) path also with subchip accuracy. The effect of multipath propagation causes severe errors in position estimation, which need to be mitigated. Moreover, the signal to noise ratio (SNR) of the received signals from the different BSs can be very low, as the MS usually communicates with one or two BSs, but needs to synchronize and track the signals of three or more BSs for positioning. In [1], T. Bertozzi analyzed a scheme for joint time delay and channel tap estimation using particle filters instead of applying a classical channel estimator. In [2], the authors analyzed adaptive tracking methods for the separation of closely spaced multipaths in the context of Rake channel estimation. J. Selva developed in [3, 4] the framework for complexity reduced maximum likelihood (ML) channel estimation (CE) methods in navigation receivers. ML CE in reduced dimension for the separation of superimposed waveforms has been analyzed with the expectation maximization (EM) algorithm in [5, 6]. The transition to parameter estimation for spread spectrum signals in mobile communications can be found as space alternating generalized expectation maximization (SAGE) in [7]. In [8], ML CE in reduced dimension for *direct sequence code dividion multiple access* (DS-CDMA) systems in mobile systems has been investigated and compared to the performance of *minimum mean square error* (MMSE) CE. In this paper, we apply different subspace methods before applying the EM and SAGE algorithm for high resolution channel parameter estimation [9] and assess their performance with respect to theoretical limits of ML CE (cf. the Cramer-Rao bound (CRB) analysis in [10], and the extensions of the CRB analysis in [6, 11] towards the Ziv-Zakai bound (ZZB)).

Notation: Vectors (e. g. $\boldsymbol{y} \in \mathbb{C}^N$) and matrices are denoted by small and captial bold letters. 'E$[\bullet]$', '$\hat{\bullet}$', 'T', '$*$', and 'H' denote the expectation, estimation, transposed, complex conjugate, and Hermitian operators. The operator '$\otimes$' expresses the calculation of the Kronecker product between two matrices. If applied to a vector $\boldsymbol{x} \in \mathbb{C}^N$, the operator $\mathrm{diag}\{\boldsymbol{x}\} \in \mathbb{C}^{N\times N}$ denotes the matrix with the elements of $\boldsymbol{x} \in \mathbb{C}^N$ on its diagonal. $\boldsymbol{y} = \mathrm{FFT}\{\boldsymbol{x}\} \in \mathbb{C}^N$ represents the fast Fourier transform (FFT) of a vector $\boldsymbol{x} \in \mathbb{C}^N$ whose dimension N is a power of 2. The i-th column of the unit matrix $1_N \in \mathbb{C}^{N\times N}$ is termed $\boldsymbol{e}_i^{(N)}$. $0_N \in \mathbb{C}^N$ represents the N-dimensional column vector with zero elements.

2. CHANNEL MODEL

In order to demonstrate the influence of the multipath propagation on the estimation performance of the LOS path and thereby on the position estimation of the MS, the channel is modelled as a fixed channel of length L

$$h(\tau,t) = h(\tau) = \sum_{\ell=1}^{L} a_\ell \delta(\tau - \tau_\ell). \tag{1}$$

where the number of channel coefficients L is assumed to be known to the receiver. The results in this paper can be considered as a worst case bound compared to the typically considered Rayleigh fading channel model, because multipath propagation undergoing Rayleigh fading always causes smaller positioning errors than fixed multipath propagation.

3. INTERPOLATION MODEL

As a pulse shape for the transmission considered in this paper, we make use of root raised cosine (RRC) pulses $g(t)$ which are defined by an one sided limit frequency f_N and a roll off factor β. We may write the direct sequence spread spectrum (DS-SS) transmit (Tx) signal as

$$\begin{aligned} s(t) = &\sum_{m=0}^{M-1} d_{\mathrm{P},m} \sum_{n=0}^{N-1} c_{\mathrm{P},n} g(t - mT - nT_\mathrm{C}), \\ &+ \sum_{m=0}^{M-1} d_{\mathrm{D},m} \sum_{n=0}^{N-1} c_{\mathrm{D},n} g(t - mT - nT_\mathrm{C}) \end{aligned} \tag{2}$$

where T and $T_\mathrm{C} = 1/R_\mathrm{C}$ denote the frame duration and chip duration with R_C being the chip rate. The pilot and data symbol sequences $d_{\mathrm{P},m}$ and $d_{\mathrm{D},m}$, $m = 0,\ldots,M-1$ are taken from

quartenary phase shift keying (QPSK) modulation. M codewords form the considered time interval for CE [12]. The spreading code sequences $c_{\mathrm{P},n}, n=0,\ldots,N-1$ for the pilots and $c_{\mathrm{D},n}, n=0,\ldots,N-1$ for the data are orthogonal Gold codes of length N in this contribution. In order to obtain a suitable matrix vector factorization beginning from Eqn. (2), we choose the sampling frequency f_{S} as integer multiple of the chip rate R_{C} yielding $Q=f_{\mathrm{S}}/R_{\mathrm{C}}$ samples per chip. If we assume an observation interval of duration MNT_{C}, we can define M successive signal vectors $\boldsymbol{s}_m \in \mathbb{C}^{NQ}$, $m=1,\ldots,M$ as $\boldsymbol{s}_m=[s[(m-1)NQ],\ldots,s[mNQ-1]]^{\mathrm{T}}$, with $s[k]=s(k/f_{\mathrm{S}})$, $k=(m-1)NQ,\ldots,mNQ-1$. Therefore, the sampled Tx signal in matrix vector notation in Eqn. (2) is $\boldsymbol{s}=[\boldsymbol{s}_1^{\mathrm{T}},\ldots,\boldsymbol{s}_M^{\mathrm{T}}]^{\mathrm{T}} \in \mathbb{C}^{MNQ}$, and $\boldsymbol{s}_m=d_{\mathrm{P},m}\boldsymbol{C}_{\mathrm{P}}\boldsymbol{g}+d_{\mathrm{D},m}\boldsymbol{C}_{\mathrm{D}}\boldsymbol{g}$, $m=1,\ldots,M$. $\boldsymbol{C}_{\mathrm{P}},\boldsymbol{C}_{\mathrm{D}} \in \mathbb{C}^{NQ\times N_{\mathrm{PP}}}$ are the pilot and data code matrices, and $\boldsymbol{g} \in \mathbb{C}^{N_{\mathrm{PP}}}$ is the zero padded sampled RRC pulse. N_{PP} is chosen as the next power of two exceeding or equal to the number of pulse samples N_{P}, for the FFT based pulse interpolation. Therefore, $\boldsymbol{g} \in \mathbb{C}^{N_{\mathrm{PP}}}$ contains the N_{P} samples of the RRC pulse padded two times with $N_{\mathrm{Z}}=(N_{\mathrm{PP}}-N_{\mathrm{P}})/2$ zeros, i. e., $\boldsymbol{g}=[0_{N_{\mathrm{Z}}}^{\mathrm{T}},g(-(N_{\mathrm{P}}-1)/(2f_{\mathrm{S}})),\ldots,g((N_{\mathrm{P}}-1)/(2f_{\mathrm{S}})),0_{N_{\mathrm{Z}}}^{\mathrm{T}}]^{\mathrm{T}}$.

The pulse interpolation enables the shifting [3]

$$\boldsymbol{g}(\tau) \approx \boldsymbol{F}^{-1}\,\mathrm{diag}\{\mathrm{FFT}\{\boldsymbol{g}\}\}\,\boldsymbol{\phi}(\tau). \tag{3}$$

The columns of $\boldsymbol{C}_{\mathrm{P}} \in \mathbb{C}^{NQ\times N_{\mathrm{PP}}}$ and $\boldsymbol{C}_{\mathrm{D}} \in \mathbb{C}^{NQ\times N_{\mathrm{PP}}}$ are circularly shifted versions of $\boldsymbol{c}_{\mathrm{P}} \otimes \boldsymbol{e}_1^{(Q)} \in \mathbb{C}^{NQ}$ and $\boldsymbol{c}_{\mathrm{D}} \otimes \boldsymbol{e}_1^{(Q)} \in \mathbb{C}^{NQ}$. The matrix $\boldsymbol{F}^{-1} \in \mathbb{C}^{N_{\mathrm{PP}}\times N_{\mathrm{PP}}}$ is the permuted inverse Fourier matrix $\left(\boldsymbol{F}^{-1}\right)_{k\ell}=\exp(\mathrm{j}\,(2\pi/N_{\mathrm{PP}})\,(k-N_{\mathrm{PP}}/2)(\ell-N_{\mathrm{PP}}/2))$, $k,\ell=1,\ldots,N_{\mathrm{PP}}$. $\boldsymbol{\phi}(\tau) \in \mathbb{C}^{N_{\mathrm{PP}}}$ is a Vandermonde vector, i. e., $(\boldsymbol{\phi}(\tau))_k=\exp(-\mathrm{j}(2\pi Q/N_{\mathrm{PP}})(k-N_{\mathrm{PP}}/2)\tau)$, $k=1,\ldots,N_{\mathrm{PP}}$.

Having determined the pulse interpolation in Eqn. (3), we can now formulate the interpolation representation of the spreading signal using the pilot and data code matrices $\boldsymbol{C}_{\mathrm{P}},\boldsymbol{C}_{\mathrm{D}} \in \mathbb{C}^{NQ\times N_{\mathrm{PP}}}$ as $\boldsymbol{s}(\tau)=[\boldsymbol{s}_1^{\mathrm{T}}(\tau),\ldots,\boldsymbol{s}_M^{\mathrm{T}}(\tau)]^{\mathrm{T}} \in \mathbb{C}^{MNQ}$, where $\boldsymbol{s}_m(\tau)=d_{\mathrm{P},m}\boldsymbol{C}_{\mathrm{P}}\boldsymbol{g}(\tau)+d_{\mathrm{D},m}\boldsymbol{C}_{\mathrm{D}}\boldsymbol{g}(\tau)=d_{\mathrm{P},m}\boldsymbol{s}_{\mathrm{P}}(\tau)+d_{\mathrm{D},m}\boldsymbol{s}_{\mathrm{D}}(\tau)$ for $m=1,\ldots,M$. $\boldsymbol{C}_{\mathrm{P}}\boldsymbol{g}(\tau)=\boldsymbol{s}_{\mathrm{P}}(\tau)$ and $\boldsymbol{C}_{\mathrm{D}}\boldsymbol{g}(\tau)=\boldsymbol{s}_{\mathrm{D}}(\tau)$ represent the interpolated pilot and data signal.

At this point it is convenient to derive a second interpolation representation for the pilot and data code $\boldsymbol{c}_P,\boldsymbol{c}_D \in \mathbb{C}^N$. The code interpolation bases on the same interpolation method as Eqn. (3). Again, the two distinct parameters are f_{N} as band limiting frequency f_{S} as sampling frequency of the RRC pulse. A Dirac delta function $\delta(t)$ which is transformed into the frequency domain, bandlimited to f_{N}, and transformed back into time domain yields the sinc function $\mathrm{sinc}(t)=\sin(2\pi f_{\mathrm{N}}t)/(\pi t)$. We proceed now in the same way as before with the interpolation of the RRC pulse: $\boldsymbol{\delta} \in \mathbb{C}^{N_{\mathrm{PP}}}$ contains the N_{P} samples of the sinc function padded two times with $N_{\mathrm{Z}}=(N_{\mathrm{PP}}-N_{\mathrm{P}})/2$ zeros to reach N_{PP}; $\boldsymbol{\delta}=[0_{N_{\mathrm{Z}}}^{\mathrm{T}},\delta(-(N_{\mathrm{P}}-1)/(2f_{\mathrm{S}})),\ldots,\delta((N_{\mathrm{P}}-1)/(2f_{\mathrm{S}})),0_{N_{\mathrm{Z}}}^{\mathrm{T}}]^{\mathrm{T}} \in \mathbb{C}^{N_{\mathrm{PP}}}$. The interpolation representation (cf. Eqn. 3) states

$$\boldsymbol{\delta}(\tau) \approx \boldsymbol{F}^{-1}\,\mathrm{diag}\{\mathrm{FFT}\{\boldsymbol{\delta}\}\}\,\boldsymbol{\phi}(\tau). \tag{4}$$

We have as interpolated pilot code $\boldsymbol{c}_{\mathrm{P}}(\tau)=\boldsymbol{C}_{\mathrm{P}}\boldsymbol{\delta}(\tau)$ and $\boldsymbol{c}_{\mathrm{D}}(\tau)=\boldsymbol{C}_{\mathrm{D}}\boldsymbol{\delta}(\tau)$ as interpolated data code.

4. TRANSMISSION MODEL

After transmission over the channel (cf. Eqn. (1)), we obtain the receive (Rx) signal vector

$$\boldsymbol{y}=\sum_{\ell=1}^{L}a_\ell\boldsymbol{s}(\tau_\ell)+\boldsymbol{n}=\boldsymbol{S}(\boldsymbol{\tau})\boldsymbol{a}+\boldsymbol{n} \in \mathbb{C}^{MNQ}, \tag{5}$$

where $n(t) \sim \mathcal{N}_{\mathrm{c}}\left(0,\sigma_n^2\right)$ describes the zero-mean additive white Gaussian noise (AWGN) of the power $\sigma_n^2=\mathrm{E}\left[|n(t)|^2\right]$, and $\boldsymbol{S}(\boldsymbol{\tau})=[\boldsymbol{s}(\tau_1),\ldots,\boldsymbol{s}(\tau_L)] \in \mathbb{C}^{MNQ\times L}$ and $\boldsymbol{a}=[a_1,\ldots,a_L]^{\mathrm{T}} \in \mathbb{C}^L$ form the signal matrix and the amplitude vector. The SNR γ is defined according to Eqn. (5) as $\gamma=\left(\sum_{\ell=1}^{L}|a_\ell|^2\right)/\sigma_n^2$.

M successive observation vectors $\boldsymbol{y}_m \in \mathbb{C}^{NQ}$ $(m=1,\ldots,M)$ form the whole observation vector $\boldsymbol{y}=[\boldsymbol{y}_1^{\mathrm{T}},\ldots,\boldsymbol{y}_M^{\mathrm{T}}]^{\mathrm{T}} \in \mathbb{C}^{MNQ}$. Therefore, the m-th observation vector $\boldsymbol{y}_m \in \mathbb{C}^{NQ}$ in Eqn. (5) is: $\boldsymbol{y}_m=\sum_{\ell=1}^{L}a_\ell\boldsymbol{s}_m(\tau_\ell)+\boldsymbol{n}_m \in \mathbb{C}^{NQ}$. Similar, we can write the noise vector as $\boldsymbol{n}=[\boldsymbol{n}_1^{\mathrm{T}},\ldots,\boldsymbol{n}_M^{\mathrm{T}}]^{\mathrm{T}} \in \mathbb{C}^{MNQ}$, $\boldsymbol{n}_m=[n((m-1)NQ/f_{\mathrm{S}},\ldots,n((mNQ-1)/f_{\mathrm{S}})]^{\mathrm{T}} \in \mathbb{C}^{NQ}$.

5. ML CHANNEL ESTIMATION IN REDUCED DIMENSION

For $\boldsymbol{y} \in \mathbb{C}^{MNQ}$, the ML estimate $\{\hat{\boldsymbol{a}},\hat{\boldsymbol{\tau}}\} \in \mathbb{C}^L$ is found according to $\{\hat{\boldsymbol{a}},\hat{\boldsymbol{\tau}}\}=\underset{\{\boldsymbol{a},\boldsymbol{\tau}\}}{\mathrm{argmin}}\|\boldsymbol{y}-\boldsymbol{S}(\boldsymbol{\tau})\boldsymbol{a}\|_2^2$. At this place, it is important to mention that the solution of the non-convex ML optimization problem refers to the tracking range $[-2T_{\mathrm{C}},2T_{\mathrm{C}}]$ [4, 13] for the estimation of the unknown channel taps $\boldsymbol{\tau} \in \mathbb{C}^L$. If there was any channel tap outside the tracking range, the system would leave the tracking range, the lock would be lost and a reacquisition procedure would be necessary. To decrease computational complexity, we propose to use the following two stage complexity reduction in Subsec. 5.1 which is also adapted to the defined tracking range to compute the ML estimate.

5.1 Bank of Correlators and Principal Components

As a first step, the pilot symbols in the sampled Rx vector $\boldsymbol{y}$ are demodulated and filtered codeword by codeword by an orthonormalized correlatorbank of N_{CC} pilot code matched correlators (CMCs) $\boldsymbol{Q}_{\mathrm{CC}} \in \mathbb{C}^{NQ\times N_{\mathrm{CC}}}$.

This matrix $\boldsymbol{Q}_{\mathrm{CC}} \in \mathbb{C}^{NQ\times N_{\mathrm{CC}}}$ is obtained from a QR decomposition of $\boldsymbol{C}_{\mathrm{CC}}=[\boldsymbol{c}_{\mathrm{P}}(\tau_{\mathrm{G},1}),\ldots,\boldsymbol{c}_{\mathrm{P}}(\tau_{\mathrm{G},N_{\mathrm{CC}}})]=\boldsymbol{Q}_{\mathrm{CC}}\boldsymbol{R}_{\mathrm{CC}}$ yielding the output of the correlatorbank as

$$\begin{aligned}\boldsymbol{y}_{\mathrm{CC}}&=\sum_{m=1}^{M}d_{\mathrm{P},m}^{*}\boldsymbol{Q}_{\mathrm{CC}}^{\mathrm{H}}\boldsymbol{y}_m=\sum_{m=1}^{M}d_{\mathrm{P},m}^{*}\boldsymbol{Q}_{\mathrm{CC}}^{\mathrm{H}}(\sum_{\ell=1}^{L}\boldsymbol{s}_m(\tau_\ell)+\boldsymbol{n}_m)\\&=M\boldsymbol{Q}_{\mathrm{CC}}^{\mathrm{H}}\sum_{\ell=1}^{L}\boldsymbol{s}_{\mathrm{P}}(\tau_\ell)+\sum_{m=1}^{M}d_{\mathrm{P},m}^{*}\boldsymbol{Q}_{\mathrm{CC}}^{\mathrm{H}}\boldsymbol{n}_m \in \mathbb{C}^{N_{\mathrm{CC}}},\end{aligned} \tag{6}$$

where we have exploited the orthogonality between the pilot CMC matrix $\boldsymbol{Q}_{\mathrm{CC}} \in \mathbb{C}^{NQ\times N_{\mathrm{CC}}}$ and the data code matrix $\boldsymbol{C}_{\mathrm{D}} \in \mathbb{C}^{NQ\times N_{\mathrm{CC}}}$. $\boldsymbol{\tau}_{\mathrm{G}}=[\tau_{\mathrm{G},1},\ldots,\tau_{\mathrm{G},N_{\mathrm{CC}}}]^{\mathrm{T}} \in \mathbb{C}^{N_{\mathrm{CC}}}$ defines the respective positions of the N_{CC} CMCs. The index represents the abbreviation Canonical Components (CCs), which is an alternative expression for signal compression using matched filter banks [13]. In the following further complexity reduction using principal components (PCs), the introduction of the filtered pilot signal

$\boldsymbol{s}_{\mathrm{P,CC}}(\tau) = \boldsymbol{Q}_{\mathrm{CC}}^{\mathrm{H}} \boldsymbol{s}_{\mathrm{P}}(\tau) \in \mathbb{C}^{N_{\mathrm{CC}}}$ is helpful. We calculate the autocorrelation matrices $\boldsymbol{R}_{\boldsymbol{s}_{\mathrm{P}}} = \mathrm{E}\left[\boldsymbol{s}_{\mathrm{P}}(\tau)\,\boldsymbol{s}_{\mathrm{P}}(\tau)^{\mathrm{H}}\right] \in \mathbb{C}^{NQ \times NQ}$ and $\boldsymbol{R}_{\boldsymbol{s}_{\mathrm{P,CC}}} = \mathrm{E}\left[\boldsymbol{s}_{\mathrm{P,CC}}(\tau)\,\boldsymbol{s}_{\mathrm{P,CC}}(\tau)^{\mathrm{H}}\right] = \boldsymbol{Q}_{\mathrm{CC}}^{\mathrm{H}} \boldsymbol{R}_{\boldsymbol{s}_{\mathrm{P}}} \boldsymbol{Q}_{\mathrm{CC}} \in \mathbb{C}^{N_{\mathrm{CC}} \times N_{\mathrm{CC}}}$ exploiting *a-priori* information about the channel taps. Here, we choose a robust *a-priori* assumption that is a uniform distribution in $[-2T_{\mathrm{C}}, 2T_{\mathrm{C}}]$ [3, 4]:

$$\boldsymbol{R}_{\boldsymbol{s}_{\mathrm{P}}} = \mathrm{E}\left[\boldsymbol{s}_{\mathrm{P}}(\tau)\,\boldsymbol{s}_{\mathrm{P}}(\tau)^{\mathrm{H}}\right] = \int_{-2T_{\mathrm{C}}}^{2T_{\mathrm{C}}} \boldsymbol{s}_{\mathrm{P}}(\tau)\,\boldsymbol{s}_{\mathrm{P}}(\tau)^{\mathrm{H}} \frac{1}{4T_{\mathrm{C}}} \mathrm{d}\tau. \tag{7}$$

For the second stage of complexity reduction, it is necessary to calculate the eigenvalue decomposition (EVD) of $\boldsymbol{R}_{\boldsymbol{s}_{\mathrm{P,CC}}} = \boldsymbol{Q}\boldsymbol{\Lambda}\boldsymbol{Q}^{\mathrm{H}}$. $\boldsymbol{Q} = [\boldsymbol{q}_1, \ldots, \boldsymbol{q}_{N_{\mathrm{CC}}}] \in \mathbb{C}^{N_{\mathrm{CC}} \times N_{\mathrm{CC}}}$ contains in its columns the respective eigenvectors and $\boldsymbol{\Lambda} = \mathrm{diag}\left\{[\lambda_1, \ldots, \lambda_{N_{\mathrm{CC}}}]^{\mathrm{T}}\right\} \in \mathbb{C}^{N_{\mathrm{CC}} \times N_{\mathrm{CC}}}$ is the diagonal matrix containing the eigenvalues sorted in descending order, i. e. $\lambda_1 > \cdots > \lambda_{N_{\mathrm{CC}}} > 0$. For a given number $N_{\mathrm{PC}} \leq N_{\mathrm{CC}}$ of PCs, the autocorrelation matrix $\boldsymbol{R}_{\boldsymbol{s}_{\mathrm{P,CC}}}$ is approximated by $\boldsymbol{R}_{\boldsymbol{s}_{\mathrm{P,CC}}} \approx \sum_{k=1}^{N_{\mathrm{PC}}} \lambda_k \boldsymbol{q}_k \boldsymbol{q}_k^{\mathrm{H}}$. As a result, we have

$$\boldsymbol{y}_{\mathrm{PC}} = \boldsymbol{Q}_{\mathrm{PC}}^{\mathrm{H}} \boldsymbol{y}_{\mathrm{CC}} \in \mathbb{C}^{N_{\mathrm{PC}}}, \tag{8}$$

where $\boldsymbol{Q}_{\mathrm{PC}} = [\boldsymbol{q}_1, \ldots, \boldsymbol{q}_{N_{\mathrm{PC}}}] \in \mathbb{C}^{N_{\mathrm{CC}} \times N_{\mathrm{PC}}}$ is the PC eigenspace matrix. At this place it is also convenient to define the twofold filtered pilot signal $\boldsymbol{s}_{\mathrm{P,PC}}(\tau) = \boldsymbol{Q}_{\mathrm{PC}}^{\mathrm{H}} \boldsymbol{Q}_{\mathrm{CC}}^{\mathrm{H}} \boldsymbol{s}_{\mathrm{P}}(\tau) \in \mathbb{C}^{N_{\mathrm{PC}}}$ needed in the following subsections.

We can now determine the ML estimate for $\boldsymbol{y}_{\mathrm{PC}}$ and $\boldsymbol{S}_{\mathrm{P,PC}}(\boldsymbol{\tau})\boldsymbol{a} \in \mathbb{C}^{N_{\mathrm{PC}}}$ ($\boldsymbol{S}_{\mathrm{P,PC}}(\boldsymbol{\tau}) = [\boldsymbol{s}_{\mathrm{P,PC}}(\tau_1), \ldots, \boldsymbol{s}_{\mathrm{P,PC}}(\tau_L)] \in \mathbb{C}^{N_{\mathrm{PC}} \times L}$) instead of $\boldsymbol{y} \in \mathbb{C}^{MNQ}$ and $\boldsymbol{S}(\boldsymbol{\tau})\boldsymbol{a} \in \mathbb{C}^{MNQ}$.

5.2 Expectation Maximization Algorithm

Alg. 1 Computation Steps for the EM Algorithm

1: Input: observation vector $\boldsymbol{y}_{\mathrm{PC}} \in \mathbb{C}^{N_{\mathrm{PC}}}$, maximum number of iterations N_{itermax}, estimation accuracy TOL,
2: initial estimations $\{\hat{\boldsymbol{\tau}}^{(0)} \in \mathbb{C}^L, \hat{\boldsymbol{a}}^{(0)} \in \mathbb{C}^L\}$, coefficients β_ℓ, $\ell = 1, \ldots, L$, iterations counter $k = 0$
3: **repeat**
4: **for** $\ell = 1, \ldots, L$ **do**
5: $\hat{\boldsymbol{x}}_\ell^{(k)} = (1 - \beta_\ell)\hat{a}_\ell^{(k)} \boldsymbol{s}_{\mathrm{P,PC}}(\hat{\tau}_\ell^{(k)}) + \beta_\ell(\boldsymbol{y}_{\mathrm{PC}} - \sum_{\ell'=1, \ell' \neq \ell}^{L} \hat{a}_{\ell'}^{(k)} \boldsymbol{s}_{\mathrm{P,PC}}(\hat{\tau}_{\ell'}^{(k)})) \in \mathbb{C}^{N_{\mathrm{PC}}}$
6: **end for**
7: **for** $\ell = 1, \ldots, L$ **do**
8: $\hat{\tau}_\ell^{(k+1)} = \underset{\tau_\ell}{\mathrm{argmax}}\{|\boldsymbol{s}_{\mathrm{P,PC}}(\tau_\ell)^{\mathrm{H}} \hat{\boldsymbol{x}}_\ell^{(k)}|^2\}$
9: $\hat{a}_\ell^{(k+1)} = \boldsymbol{s}_{\mathrm{P,PC}}(\hat{\tau}_\ell^{(k+1)})^{\mathrm{H}} \hat{\boldsymbol{x}}_\ell^{(k)} / \|\boldsymbol{s}_{\mathrm{P,PC}}(\hat{\tau}_\ell^{(k+1)})\|_2^2$
10: **end for**
11: $k \rightarrow k+1$
12: **until** $\|\hat{\boldsymbol{\tau}}^{(k)} - \boldsymbol{\tau}\|_2^2 + \|\hat{\boldsymbol{a}}^{(k)} - \boldsymbol{a}\|_2^2 <$ TOL or $k > N_{\mathrm{Itermax}}$

Alg. 1 sums up the different steps belonging to the EM algorithm. All pairs of channel parameters $\{\tau_\ell, a_\ell\}$, $\ell = 1, \ldots, L$ are estimated in parallel beginning with some initial estimates $\hat{\boldsymbol{\tau}}^{(0)} = [\hat{\tau}_1^{(0)}, \ldots, \hat{\tau}_L^{(0)}]^{\mathrm{T}} \in \mathbb{C}^L$ and $\hat{\boldsymbol{a}}^{(0)} = [\hat{a}_1^{(0)}, \ldots, \hat{a}_L^{(0)}]^{\mathrm{T}} \in \mathbb{C}^L$ for the channel taps and amplitudes. We observe the typical structure with the expectation (E) step (line 5) followed by the maximization (M) step (lines 8 to 9).

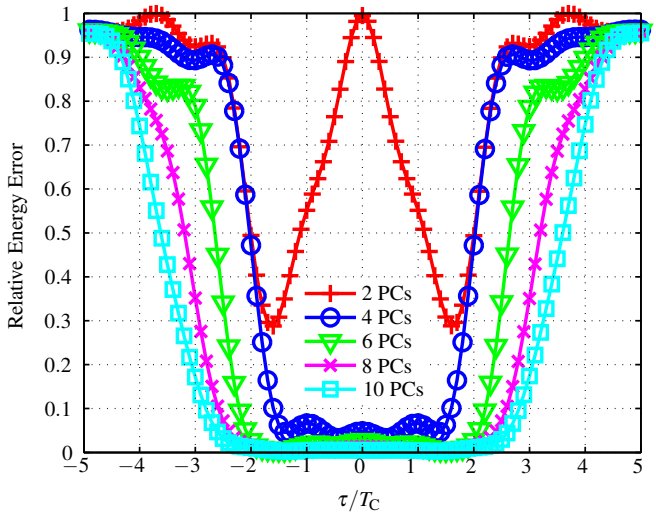

Figure 1: CMC and PC Compression Quality

The iterative parallel estimation of $\{\tau_\ell, a_\ell\}$, $\ell = 1, \ldots, L$ is repeated until a required estimation accuracy is achieved or the maximum number of iterations N_{Itermax} is exceeded.

5.3 Space Alternating Generalized Expectation Maximization Algorithm

Alg. 2 Computation Steps for the SAGE Algorithm

1: Input: observation vector $\boldsymbol{y}_{\mathrm{PC}} \in \mathbb{C}^{N_{\mathrm{PC}}}$, maximum number of iterations N_{itermax}, estimation accuracy TOL,
2: initial estimations $\{\hat{\boldsymbol{\tau}}^{(0)} \in \mathbb{C}^L, \hat{\boldsymbol{a}}^{(0)} \in \mathbb{C}^L\}$, iterations counter $k = 0$
3: **repeat**
4: **for** $\ell = 1, \ldots, L$ **do**
5: $\hat{\boldsymbol{x}}_\ell^{(k)} = \boldsymbol{y}_{\mathrm{PC}} - \sum_{\ell'=1}^{\ell-1} \hat{a}_{\ell'}^{(k+1)} \boldsymbol{s}_{\mathrm{P,PC}}(\hat{\tau}_{\ell'}^{(k+1)}) - \sum_{\ell'=\ell+1}^{L} \hat{a}_{\ell'}^{(k)} \boldsymbol{s}_{\mathrm{P,PC}}(\hat{\tau}_{\ell'}^{(k)}) \in \mathbb{C}^{N_{\mathrm{PC}}}$
6: $\hat{\tau}_\ell^{(k+1)} = \underset{\tau_\ell}{\mathrm{argmax}}\{|\boldsymbol{s}_{\mathrm{P,PC}}(\tau_\ell)^{\mathrm{H}} \hat{\boldsymbol{x}}_\ell^{(k)}|^2\}$
7: $\hat{a}_\ell^{(k+1)} = \boldsymbol{s}_{\mathrm{P,PC}}(\hat{\tau}_\ell^{(k+1)})^{\mathrm{H}} \hat{\boldsymbol{x}}_\ell^{(k)} / \|\boldsymbol{s}_{\mathrm{P,PC}}(\hat{\tau}_\ell^{(k+1)})\|_2^2$
8: **end for**
9: $k \rightarrow k+1$
10: **until** $\|\hat{\boldsymbol{\tau}}^{(k)} - \boldsymbol{\tau}\|_2^2 + \|\hat{\boldsymbol{a}}^{(k)} - \boldsymbol{a}\|_2^2 <$ TOL or $k > N_{\mathrm{Itermax}}$

Alg. 2 shows the successive steps belonging to the SAGE algorithm. Contrary to the EM algorithm, all pairs of channel parameters are estimated sequentially, and again, we can observe in line 5 the E step and in line 6 and 7 the M step. This iterative estimation is repeated at most N_{Itermax} times or is stopped earlier if a required accuracy is already reached.

6. SIMULATIONS AND RESULTS

The simulations for the reduced complexity ($N_{\mathrm{CC}} = 40$ CMCs with spacing $1/f_{\mathrm{S}}$ and successive $N_{\mathrm{PC}} = 20$ PCs) estimation of a $L = 2$ tap channel ($\{a_1 = 1, \tau_1 = -0.1 \cdot T_{\mathrm{C}}\}$ and $\{a_2 = 1/\sqrt{2}, \tau_2 = 0.3 \cdot T_{\mathrm{C}}\}$) are the averaged result over $N_{\mathrm{Channel}} = 10000$ random channel realizations. The quality of the complexity reduction is shown in Fig. 1. We see that within the considered delay interval $[-2T_{\mathrm{C}}, 2T_{\mathrm{C}}]$,

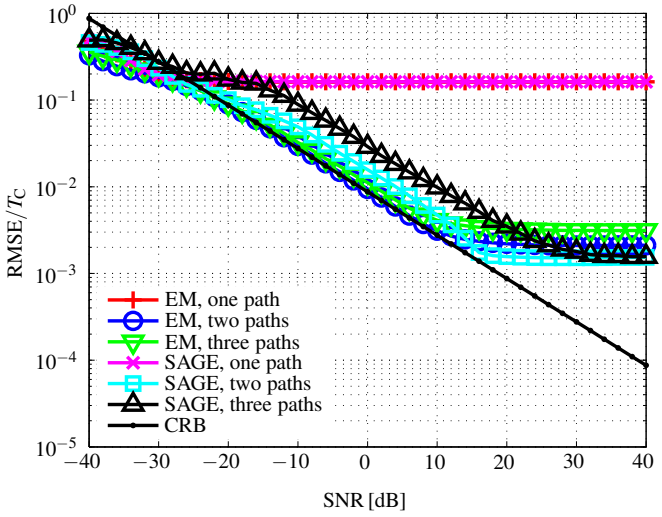

Figure 2: RMSE of LOS Path Estimation Versus the SNR for Different Estimation Algorithms and Degrees of Freedom

the relative energy error $\|\boldsymbol{P}_{\mathrm{PC}}\boldsymbol{s}_{\mathrm{P}}(\tau)\|_2^2 / \|\boldsymbol{s}_{\mathrm{P}}(\tau)\|_2^2$ is approximately zero. The orthonormal projection matrix $\boldsymbol{P}_{\mathrm{PC}} = 1_{NQ} - \boldsymbol{Q}_{\mathrm{CC}}\boldsymbol{Q}_{\mathrm{PC}}\boldsymbol{Q}_{\mathrm{PC}}^{\mathrm{H}}\boldsymbol{Q}_{\mathrm{CC}}^{\mathrm{H}}$ projects onto the orthonormal complement of the CMC correlator bank and the PCs. Previous investigations in [13] showed that the loss in estimation accuracy with respect to the root mean square error (RMSE) is proportional to $1/\left(1-\|\boldsymbol{P}_{\mathrm{PC}}\boldsymbol{s}_{\mathrm{P}}(\tau)\|_2^2/\|\boldsymbol{s}_{\mathrm{P}}(\tau)\|_2^2\right) \approx 1$. Therefore, the choice of the investigated complexity reduction allows us to restrict the further simulation results to the consideration of the reduced complexity implementations. All other parameters according to [12] are listed in Tab. 1, which are typically for a UMTS system. In the resulting plot in Fig. 2, which shows the RMSE $\sqrt{\mathrm{E}\left[|\hat{\tau}_1-\tau_1|^2\right]}/T_{\mathrm{C}}$ of the LOS path estimation for the SNR range between -40 dB and 40 dB, we can see the performance of the LOS path and therefore the position estimation of the two complexity reduced implementations with different degrees of freedom. The results are compared to the theoretical optimum performance for unbiased estimators, the CRB. We observe that the two estimators with degree one show the bias due to the multipath propagation, even at very high SNR values. The consecutive position error would be at about 40 m. Therefore, a precise position estimation requires more than one degree of freedom in the optimization. If we resort to the two and three path EM algorithm, the CRB can be approximated very closely within the medium SNR range. Contrary, the SAGE algorithm shows a slight more adaption to the noise in the SNR range between -25 dB and 15 dB. Another important observation in Fig. 2 is the saturation of the RMSE values for SNR values above 10 dB shown by the two and three path estimators, which is due to EM and SAGE related solutions of the ML estimation problem. We would observe this saturation effect also for the EM and SAGE algorithm without complexity reduction. In Subsec. 5.1, we have already shown that the complexity reduction only leads to a slightly increased variance, and not to any bias which is responsible for saturation effects. On the one hand, the RMSE curves saturate at a high SNR and on the other the CRB is crossed at very low SNR. The RMSE curves show a saturation at a value of about 0.5 m for increasing SNR which is a quite precise position determination. We can give two possible explanations for RMSE values which are below the CRB for low SNR values. As a first reason, we resort to the limited tracking range defined at the beginning in Sec. 5. The ML search within the defined tracking range in line 8 of Alg. 1 and line 6 of Alg. 2 is implemented by means of a onedimensional Newton algorithm. The suggested Newton optimization methods require the limitation to a certain search range which is set to the considered tracking range. Once the noise is too high, the RMSE saturates and cannot follow the theoretical CRB any more. The second reason follows the observations in [9] and explains why in [6, 11], the CRB was extended towards the ZZB. Once the noise power exceeds a certain level, the estimation algorithms for $L=1$, $L=2$ or $L=3$ undergo a model mismatch, because this high noise power would require to estimate an infinite number of paths. The hypothesis test for the discrimination of different channel lengths L suggested in [13] also confirms these observations. This test bases on the evaluation of several log-likelihood functions choosing the respective one with the least likelihood value. Clearly, a too high noise level affects the respective function values and may therefore degrade the testing performance substantially.

parameter	value
roll off factor (RRC pulse):	$\beta = 0.22$
one sided limit frequency (RRC pulse):	$f_{\mathrm{N}} = 5\,\mathrm{MHz}$
physical sampling frequency:	$f_{\mathrm{S}} = 20$ MHz
chip rate:	$R_{\mathrm{C}} = 4\,\mathrm{MHz}$
code length (Gold code):	255
number of pulse samples:	$N_{\mathrm{P}} = 55$
number of transmitted pilots:	$M = 10$

Table 1: List of Used Simulation Parameters

7. COMPUTATIONAL COMPLEXITY

The following complexity analysis counts both one complex addition as well as one complex multiplication as one floating point operation (FLOP). Tab. 2 list the computational complexity of the EM and SAGE algorithm with and without the suggested complexity reduction methods. The above half of Tab. 2 shows the computational complexity of the E and M step necessary to implement the EM and SAGE algorithms. This complexity is due to the correlation of spreading sequences of length NQ. If we consider the computational complexity of the implementation of the compressed signals in the below half of Tab. 2, the complexity of the correlation only depends on N_{PC}. As additional *a-priori* complexity, we have for the CC analysis $\mathrm{O}\left(NQ(N_{\mathrm{CC}})^2\right)$ and $\mathrm{O}\left((N_{\mathrm{CC}})^2 N_{\mathrm{PC}}\right)$ for the PC decomposition, respectively. Dependend on the channel length L and on the needed number of iterations $N_{\mathrm{Iterations}}$ until convergence, we obtain for the assumed parameter values a maximum complexity of $L \cdot N_{\mathrm{Iterations}} \cdot 10^7$ complex flops, but for the implementation resorting to the two steps of complexity decreasing, $L \cdot 2 \cdot N_{\mathrm{Iterations}} \cdot 10^5 + 5 \cdot 10^6$ complex flops suffice. Therefore, the proposed CC and PC algorithms allowed to decrease the computational complexity of the whole simulation at least by a factor of 2 for $L=1$ and $N_{\mathrm{Iterations}} = 1$. This gain increases for a growing model order L and an increasing number of iterations $N_{\mathrm{Iterations}}$. Fig. 3 shows the average number of iterations $N_{\mathrm{Iterations}}$ for the investigated estimation algorithms for the respective degrees of freedom dependend on the SNR. We see that the biased estimators for $L=1$ converge after two iterations to the ML solution independend of

	EM or SAGE without CC and PC method
E and M step	$((L+1)NQ+1)N_{\text{Itermax}}N_{\text{Channel}}$
	EM or SAGE with CC and PC method
E and M step	$((L+1)N_{\text{PC}}+1)N_{\text{Itermax}}N_{\text{Channel}}$
$\boldsymbol{Q}_{\text{CC}}$	$\text{O}\left(NQ\left(N_{\text{CC}}\right)^2\right)$
EVD of $\boldsymbol{R}_{\boldsymbol{s}_{\text{CC}}}$	$\text{O}\left(\left(N_{\text{CC}}\right)^2 N_{\text{PC}}\right)$

Table 2: Computational Complexity for EM and SAGE Implementations Before and After Complexity Reduction

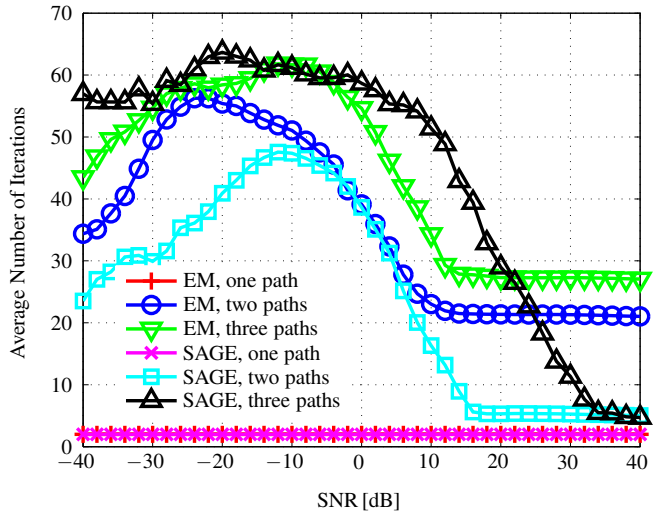

Figure 3: Average Number of Iterations Versus the SNR for Different Estimation Algorithms and Degrees of Freedom

the respective SNR value. Contrary, for $L=2$ the advantages of the SAGE implementation compared to EM algorithm become clear. The number of iterations can be decreased substantially by the sequential (SAGE) and not the parallel (EM) estimation procedure, especially for very low and very high SNR values. For a too high model order of $L=3$, this effect is only still true for a very low noise power. This observation fits the RMSE plot in Fig. 2, because in the medium SNR range of $-25\,\text{dB}$ to $15\,\text{dB}$, the SAGE algorithm for $L=3$ degrees of freedom showed an adaption to the noise in the form of an increased RMSE, leading to a worse convergence behaviour. It is also important to mention that for exteme high SNR values above $35\,\text{dB}$, the number of needed iterations does not depend any more on the model order L of the estimation algorithm for sequential SAGE estimator.

8. CONCLUSIONS

This contribution dealt with complexity reduced approaches for maximum likelihood (ML) channel estimation (CE) in reduced dimensions. The tremendous complexity reduction was achieved using a bank of code matched correlators (CMCs) followed by the standard principal component (PC) approach. Previous investigations had shown that a direct PC application is optimum with respect to energy compression error and estimation bias. However, the CMC prefiltering before was necessary for two reasons: on the one hand for the separation of superimposed orthogonal spreading sequences in the receiver, and on the other, a direct PC filtering would require too much computational complexity. The CMC and PC filtering matrices have been calculated in advance, and the iterative ML CE has been implemented resorting to compressed observation and signal vectors. Simulation results showed that the positioning bias introduced by the chosen complexity reduction is less than $0.5\,\text{m}$ in a UMTS scenario. Therefore, we have designed a variant of expectation maximization (EM) and space alternating generalized expectation maximization (SAGE) based ML CE fitting especially mass market receivers with critical signal processing complexity.

REFERENCES

[1] T. Bertozzi, D. Le Ruyet, C. Panazio, and H. Vu Thien, "Channel Tracking Using Particle Filters in Unresolvable Multipath Environments," *EURASIP Journal on Applied Signal Processing*, vol. 15, pp. 2328–2338, 2004.

[2] G. Fock, J. Baltersee, P. Schulz-Rittich, and H. Meyr, "Channel Tracking for Rake Receivers in Closely Spaced Multipath Environments," *IEEE Journal on Selected Areas in Communications*, vol. 19, no. 12, pp. 2420–2431, December 2001.

[3] J. Selva, "Complexity Reduction in the Parametric Estimation of Superimposed Signals," *Signal Processing*, vol. 84, pp. 2325–2343, 2004.

[4] J. Selva, "An Efficient Newton-Type Method for the Computation of ML Estimators in a Uniform Linear Array," *IEEE Transactions on Signal Processing*, vol. 53, no. 6, pp. 2036–2045, 2005.

[5] M. Feder and E. Weinstein, "Parameter Estimation of Superimposed Signals Using the EM Algorithm," *IEEE Transactions on Acoustics, Speech, and Signal Processing*, April 1988.

[6] A. Weiss and E. Weinstein, "Fundamentals in Passive Time Delay Estimation-Part i: Narrow-Band Systems," *IEEE Transactions on Acoustics, Speech, and Signal Processing*, vol. 31, no. 2, April 1983.

[7] B. Fleury, M. Tschudin, R. Heddergott, D. Dalhaus, and K. I. Pedersen, "Channel Parameter Estimation in Mobile Radio Environments using the SAGE Algorithm," *IEEE Journal on Selected Areas in Communications*, March 1999.

[8] F. Dietrich and W. Utschick, "Pilot-Assisted Channel Estimation Based on Second-Order Statistics," *IEEE Transactions on Signal Processing*, vol. 53, no. 3, March 2005.

[9] M. Tschudin, *Analyse und Vergleich von hochauflösenden Verfahren zur Funkkanalparameterschätzung*, Ph.D. thesis, Swiss Federal Institute of Technology, Zurich, Switzerland, 1999.

[10] J. Soubielle, I. Fijalkow, P. Duvaut, and A. Bibaut, "GPS Positioning in a Multipath Environment," *IEEE Transactions on Signal Processing*, vol. 50, no. 1, pp. 141–150, January 2002.

[11] J. Ziv and M. Zakai, "Some Lower Bounds on Signal Parameter Estimation," *IEEE Transactions on Information Theory*, vol. 15, no. 3, May 1969.

[12] *3GPP Technical Specification Group Radio Access Network, UE Radio Transmission and Reception (FDD), 3G TS 25.101 Version*, December 2000.

[13] J. Selva, *Efficient Multipath Mitigation Methods in Navigation Systems*, Ph.D. thesis, Universitat Polytecnicia de Catalunya, Barcelona, Spain, 2004.